X-Ray Scattering Study of the Surface Morphology of Au(111) during Ar^+ Ion Irradiation

M. V. Ramana Murty, T. Curcic, A. Judy, and B. H. Cooper
Laboratory of Atomic and Solid State Physics, Cornell University, Ithaca, New York 14853

A. R. Woll and J. D. Brock
School of Applied and Engineering Physics, Cornell University, Ithaca, New York 14853

S. Kycia and R. L. Headrick
Cornell High Energy Synchrotron Source (CHESS), Wilson Laboratory, Ithaca, New York 14853
(Received 3 October 1997)

Using real-time x-ray scattering to measure the surface morphology of Au(111) during sputter erosion with 500 eV Ar^+ ions, we observe three distinct regimes: three-dimensional rough erosion at 20–60 °C, quasi-layer-by-layer removal at 120–220 °C, and step retraction above 270 °C. Sputtering at 20–60 °C leads to pattern formation with a characteristic spacing between features. The average separation l between features increases with time t, consistent with a power law $l \sim t^{0.27\pm0.02}$. The observations are consistent with the predictions of a continuum model for *deposition* which includes an Ehrlich-Schwoebel barrier to the interlayer diffusion of surface defects. [S0031-9007(98)06122-5]

PACS numbers: 68.35.Bs, 61.10.Eq, 61.80.Jh, 79.20.Rf

Ion beam sputtering is frequently employed for patterning of surfaces, surface cleaning, and depth profiling. Sputtered surfaces display a variety of morphologies depending on the sputtering geometry and the surface defect kinetics. A ripple pattern was observed on SiO_2 and Ge(001) with 1 keV Xe^+ ions incident at 55° with respect to the surface normal, and was attributed to the curvature dependence of the sputter yield [1,2]. A similar pattern on Ag(110) formed by Ar^+ ions (energies > 800 eV) at normal incidence was ascribed to the anisotropic diffusion of surface defects [3]. On the other hand, sputtering of Cu(001) at room temperature with 400 eV Ar^+ ions [4], Pt(111) at 352 °C with 600 eV Ar^+ ions [5], and Ge(001) at 295 °C with 240 eV Xe^+ ions [6] led to a pattern of pits and mounds. Our goal in this work is to investigate the scaling behavior of parameters that characterize the surface morphology during ion irradiation. The study of dynamic scaling can elucidate the dominant roughening and smoothing mechanisms on the surface. Compared to thin film growth, few studies have investigated scaling relations during sputtering [6,7].

In this Letter, we report results from real-time x-ray scattering measurements of the evolution of surface morphology during erosion of Au(111) with 500 eV Ar^+ ions. We observe three-dimensional rough erosion at 20–60 °C, marked by the formation of features with a characteristic spacing. The average separation l of the features evolves with time t, consistent with a scaling relation $l \sim t^{0.27\pm0.02}$. The aspect ratio of the features, assumed to be close packed [5,6], remains nearly constant as they evolve. The observations are consistent with the predictions of a continuum model for *deposition* which includes an Ehrlich-Schwoebel barrier [8] to the interlayer diffusion of surface defects. At intermediate temperatures, from 120–220 °C, quasi-layer-by-layer sputtering is observed, while step retraction is observed above 270 °C.

The x-ray scattering experiments were performed with 10 keV x rays at the Cornell High Energy Synchrotron Source (CHESS). The chamber base pressure was less than 5×10^{-10} mbar. The Ar^+ ion energy was 500 eV, and the ions were incident at 45° with respect to the surface normal. The background pressure of Ar was 10^{-5}–10^{-4} mbar during Ar^+ ion irradiation. Temperatures in the 100–220 °C range were measured with an infrared pyrometer, and temperatures outside this range with a thermocouple calibrated against the pyrometer. The Au(111) single crystal, with a miscut of less than 0.1°, was prepared by sputtering and annealing at 350 °C. No contaminants were detected on the freshly prepared surface using Auger electron spectroscopy. Low-energy electron diffraction (LEED) from the surface, performed in a separate chamber, showed the $22 \times \sqrt{3}$ reconstruction on the well-annealed surface [9].

In situ x-ray scattering was performed using a custom diffractometer [10]. The experiments described below involve *real-time* measurements of the specular beam intensity and off-specular diffuse scattering in transverse scans through the $(0\ 0)_{\mathrm{hex}}$ truncation rod. The subscript hex refers to the description of the fcc crystal using hexagonal lattice basis vectors [9]. In the following, $q_\perp$ and $q_\parallel$ refer to the normal and in-plane components of the scattering vector, and d is the spacing between adjacent $(111)_{\mathrm{cubic}}$ planes in the bulk. Real-space directions are indicated in the conventional simple cubic representation.

Figure 1(a) shows the normalized specular beam intensity at the $(0\ 0\ 1.44)_{\mathrm{hex}}$ position, close to the anti-Bragg $[(0\ 0\ 1.5)_{\mathrm{hex}}, q_\perp d = \pi]$ position, during Ar^+ ion irradiation on Au(111). Three distinct sputter regimes were observed. At 270 °C, the intensity stays essentially

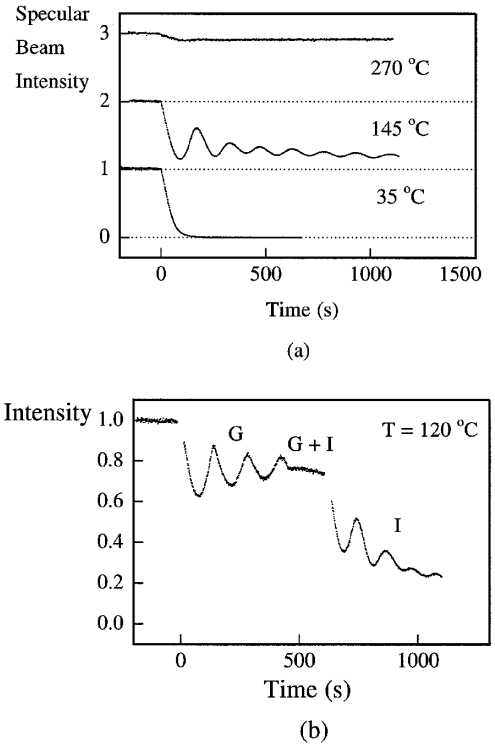

FIG. 1. (a) Normalized specular beam intensity at the $(0\ 0\ 1.44)_{\mathrm{hex}}$ position during sputtering at different temperatures. The data at different temperatures are offset vertically for clarity. (b) Normalized specular beam intensity during a sequence of growth (G), simultaneous growth and ion irradiation ($G + I$), and ion irradiation alone (I).

constant, indicating material removal by step retraction. At 145 °C, we observe intensity oscillations, suggesting quasi-layer-by-layer removal [11]. The intensity oscillations are caused by the nucleation, growth, and coalescence of two-dimensional islands of surface vacancies. The amplitude of the oscillations decays rapidly, suggesting imperfect layer-by-layer removal. Such layer-by-layer removal with energetic ions has been previously observed on Pt(111), Si(111), and Si(001) [13,14] and in STM studies on Au(111) [15,16].

Sputtering at 35 °C results in a rapid decay of the specular beam intensity at the anti-Bragg position, as shown in Fig. 1(a). Off-specular diffuse scattering observed in transverse scans through the $(0\ 0\ 0.18)_{\mathrm{hex}}$ position gives information about the positional and orientational correlations between surface features. Figure 2(a) shows the scattered intensity vs $q_{\parallel}$, taken *during* Ar^+ ion irradiation at 35 °C. The sputter rate was 140 s/ML, and the ions were incident along an azimuth 39° from the surface $\langle \bar{1}10\rangle_{\mathrm{cubic}}$ axis. The asymmetry in the reflectivity curves at early times is due to the rapidly changing dimensions of surface features during a single scan, which took about three minutes. Scans taken after removal of 5 monolayers (ML) were approximately symmetric about $(0\ 0\ 0.18)_{\mathrm{hex}}$. Satellite peaks on either side of the specular peak indicate a characteristic lateral length scale on the surface. The position of the satellite peaks was found to be essentially independent of $q_{\perp}$ in the range $q_{\perp}d = 0.12\pi$ to 0.25π, showing that these peaks are not due to specular reflection from facets. Figure 2(b) shows contours of constant intensity in the diffuse scattering over an azimuthal range of 120°. The satellite peak forms a ring (Henzler ring [17]) around the specular beam, and its radial position is nearly independent of azimuth, ruling out a pattern of unidirectional ripples as observed in Refs. [1–3]. Local maxima in the Henzler ring along the $(0\bar{1}0)_{\mathrm{hex}}$

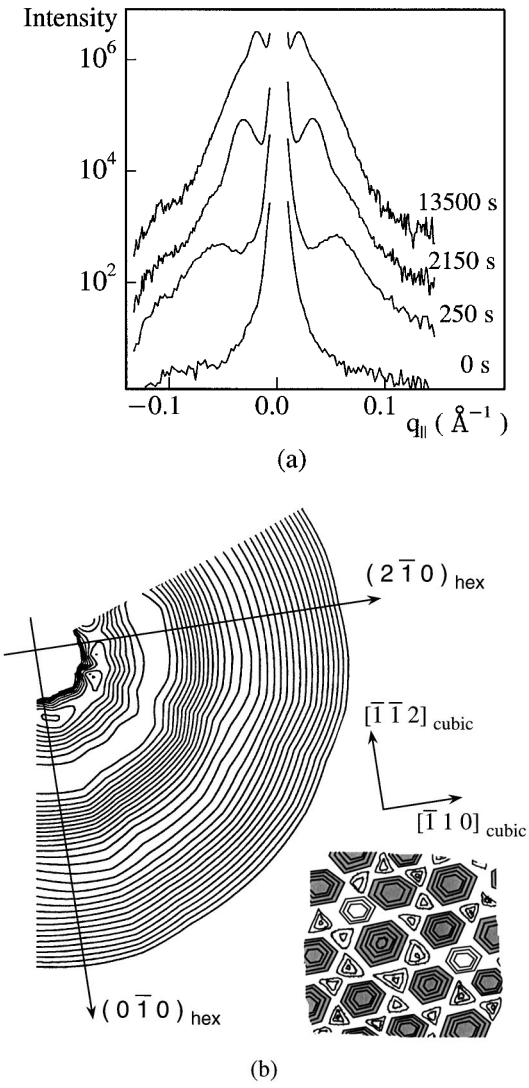

FIG. 2. (a) Off-specular diffuse scattering in transverse scans through $(0\ 0\ 0.18)_{\mathrm{hex}}$ during 500 eV Ar^+ ion irradiation at 35 °C. The scans have been offset vertically for clarity. (b) Contours of constant intensity (equal increments on logarithmic scale) over a range of azimuthal angles spanning 120° after removal of ≈70 ML. The specular peak is not shown. Radial scans were taken at intervals of 10° in azimuth. The satellite peak appears at approximately the same radial position at all azimuths. The Henzler ring has local maxima along $(0\bar{1}0)_{\mathrm{hex}}$ and $(1\bar{1}0)_{\mathrm{hex}}$ directions. Inset: Schematic of the surface covered with pits (shaded) and mounds with orientations indicated by the x-ray and LEED measurements. We note that the local order is exaggerated and that there is a size distribution of objects on the surface.

and $(1\bar{1}0)_{\text{hex}}$ directions indicate that vectors joining the centers of nearest neighbor objects are more likely to lie along surface $\langle\bar{1}10\rangle_{\text{cubic}}$ directions [see Fig. 2(b) inset]. We performed LEED measurements of Au(111) irradiated with 500 eV Ar^+ ions at room temperature and observed streaks consistent with small facets. This LEED observation is consistent with STM observations of vacancy islands bounded by $\langle\bar{1}10\rangle_{\text{cubic}}$ steps on an ion irradiated Au(111) surface [15]. The x-ray data are consistent with the surface being covered with three-dimensional pits and mounds [5] shown schematically in the inset in Fig. 2(b).

The satellite peaks move to smaller $q_{\parallel}$ as sputtering continues, indicating a separation between features that increases with time. This can occur through the coalescence of neighboring features as they grow. In view of the sharpness of the satellite peaks, we make a simple estimate of the average separation between features from $l \approx 4\pi/\delta q_{\parallel}$, where $\delta q_{\parallel}$ is the separation between satellite peaks. Figure 3 shows the variation of l with the number of monolayers removed for three different substrate temperatures at a sputter rate of 140 s/ML and for two different sputter rates at 35 °C. Over the range of our data, the evolution of the average separation between features is consistent with a power law $l \sim t^{0.27\pm0.02}$. We note that only data taken after removal of ≈10 ML was considered for the fit. For the same ion dose, the length scale is seen to increase with temperature. This is expected due to the longer diffusion length of a surface vacancy at the higher temperature (or, similarly, to the faster rate of detachment and diffusion of adatoms to fill a surface vacancy). A similar argument explains the longer length scale observed with the lower flux at 35 °C. A quantitative analysis of the observed line shapes, using a distribution function of feature sizes and separations, yields the same coarsening exponent and is the subject of a separate paper [18].

A measure of the aspect ratio of the surface features, assumed to be close packed [5,6], is the ratio of interface width w to the average separation between features. The interface width can be estimated from $I(q_\perp) = I_0(q_\perp)\exp(-q_\perp^2 w^2)$, where $I(q_\perp)$ and $I_0(q_\perp)$ are the specular beam intensities on the etched and the starting surface, respectively [19,20]. The inset of Fig. 3 shows the evolution of the ratio w/l as a function of material removed at 35 °C. The ratio very quickly reaches a value of ≈0.025 and stays nearly constant throughout the sputtering time. Thus the features maintain a nearly constant aspect ratio as they evolve, often taken to indicate slope selection for the sides of the pits and mounds [21].

The coarsening exponent of 0.27 ± 0.02 is close to the predicted value of 0.25 in a continuum model for mound formation in molecular beam epitaxy (MBE) [8]. An Ehrlich-Schwoebel barrier to the interlayer diffusion of adatoms can give rise to mounds with a characteristic spacing in MBE [21–24]. In an analogous way, but with vacancies as the mobile species, an Ehrlich-Schwoebel barrier for vacancies can give rise to pattern formation during sputtering. There are at least two other mechanisms that can give rise to the observed pattern during sputtering. The first is a vacancy-step attraction [25]. The other, with adatoms as the mobile species, is an Ehrlich-Schwoebel barrier for thermally generated adatoms to fill a vacancy. The present measurements do not distinguish between the various mechanisms.

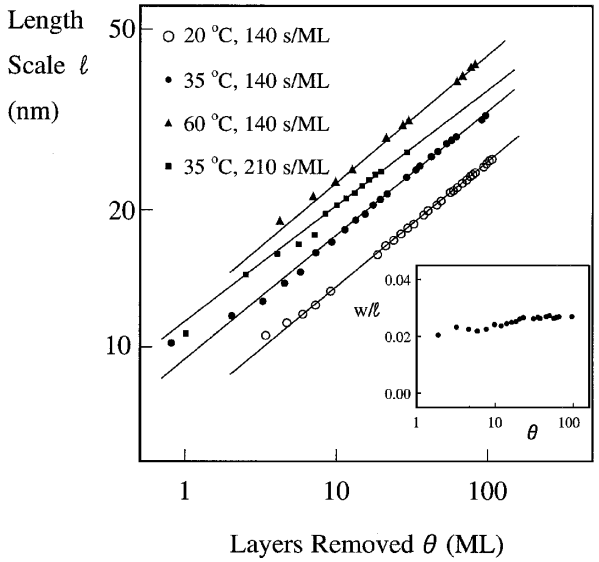

FIG. 3. Variation of the average separation l between pits with the number of monolayers removed θ for three different substrate temperatures at 140 s/ML and two different sputter rates at 35 °C. The solid lines $l \sim \theta^n$ are least squares fits to the data (only points after removal of 10 ML were considered in the fit) and give $n = 0.27 \pm 0.02$. Inset: Variation of w/l as a function of the number of monolayers removed at 35 °C, where w is the interface width.

In the context of sputtering, the continuum model in Ref. [8] expresses the rate of change of height h at a point on the surface in terms of (a) the downhill current $\mathbf{j}_s$ of surface vacancies driven by the Ehrlich-Schwoebel barrier ($\nabla \cdot \mathbf{j}_s$), (b) a noise term describing the random production of vacancies, and (c) a surface diffusion-mediated relaxation term ($\nabla^4 h$). The coarsening exponent of 0.25 requires atom detachment from steps to occur at a sufficiently fast rate so that the $\nabla^4 h$ term is significant in relation to the other terms [21,26]. In our experiments, when ion irradiation was stopped, significant smoothing of the surface was observed on the time scale of the removal of 1 ML [27]. Hence, atom detachment from steps plays a significant role in the evolving surface morphology during sputtering. The observation of slope selection suggests that there is an uphill current to balance the downhill current of vacancies at the selected slope. An uphill current can arise from surface relaxation driven by line tension [26] or from a transient mobility of vacancies after an ion impact. In the latter mechanism, the energy deposited in the lattice by an ion incident near a step edge can lead to an enhanced hopping of vacancies (and adatoms) across the step edge. Such

an enhanced interlayer diffusion will increase with an increase in step density. This mechanism is similar to the proposed downward funneling mechanism for adatoms during epitaxy on bcc/fcc (001) surfaces [28,29].

Finally, Fig. 1(b) shows specular beam intensity measured during growth (G), irradiation (I), and simultaneous growth and irradiation ($G + I$) at 120 °C [14]. Note that, at this temperature, both the growth and irradiation are in the layer-by-layer regime. The growth oscillations show cusps and the (normalized) intensity maxima rise almost up to unity, indicating nearly ideal layer-by-layer growth. The oscillations during irradiation alone are less ideal. Note also that the period of the oscillations during irradiation is less than that during growth; if we assume that the amount of material deposited in one growth oscillation is 1 ML, the amount of material removed during each sputter oscillation corresponds to 0.90 ± 0.05 ML [30]. Such a reduction in the period of oscillations has been predicted for systems where surface defects (adatoms/vacancies) face an Ehrlich-Schwoebel barrier [31]. In a simple picture, when the vacancy islands, separated by an average distance L, reach a critical size $R_c < L$, second layer nucleation becomes highly likely and most new vacancies created go into the second layer [32]. The preferred attachment of vacancies to the second layer causes the specular beam intensity to turn around at a coverage $\theta < 1$ (provided $\theta > 0.5$).

In conclusion, we have observed pattern formation and quasi-layer-by-layer sputtering during 500 eV Ar^+ ion irradiation on Au(111). Both an Ehrlich-Schwoebel barrier to the interlayer diffusion of surface defects (adatoms/vacancies) and a vacancy-step attraction could give rise to these phenomena. The power law $l \sim t^{0.27\pm0.02}$ describing the evolution of the average separation between features with time, is consistent with a theoretical model [8] that includes an Ehrlich-Schwoebel barrier to the interlayer diffusion of surface defects.

This work was supported by the Cornell University Materials Science Center under Grant No. NSF-DMR-9632275 and by the AFOSR under Grant No. F49620-97-1-0020. Part of this work was conducted at CHESS which is supported by the NSF under Grant No. DMR-9311772.

[1] E. Chason *et al.,* Phys. Rev. Lett. **72**, 3040 (1994).
[2] T. M. Mayer *et al.,* J. Appl. Phys. **76**, 1633 (1994).
[3] S. Rusponi *et al.,* Phys. Rev. Lett. **78**, 2795 (1997).
[4] M. Ritter *et al.,* Surf. Sci. **348**, 243 (1996); H.-J. Ernst, Surf. Sci. **383**, L755 (1997).
[5] T. Michely and G. Comsa, Nucl. Instrum. Methods Phys. Res., Sect. B **82**, 207 (1993).
[6] S. J. Chey *et al.,* Phys. Rev. B **52**, 16 696 (1995).
[7] E. A. Eklund *et al.,* Phys. Rev. Lett. **67**, 1759 (1991).
[8] M. Siegert and M. Plishcke, Phys. Rev. Lett. **73**, 1517 (1994).
[9] A. R. Sandy *et al.,* Phys. Rev. B **43**, 4667 (1991); J. V. Barth *et al.,* Phys. Rev. B **42**, 9307 (1990).
[10] R. L. Headrick *et al.,* Phys. Rev. B **54**, 14 686 (1996).
[11] A change in the coverage of surface reconstruction can also influence the specular beam intensity (Refs. [9,12]). However, this effect is too small to account for the amplitude of the intensity oscillations.
[12] P. Bedrossian (private communication).
[13] B. Poelsema *et al.,* Phys. Rev. Lett. **53**, 2500 (1984).
[14] P. Bedrossian *et al.,* Phys. Rev. Lett. **67**, 124 (1991); P. Bedrossian and T. Klitsner, Phys. Rev. B **44**, 13 783 (1991).
[15] T. Michely *et al.,* Surf. Sci. **230**, L135 (1990).
[16] K. P. Reimann *et al.,* Mater. Res. Soc. Symp. Proc. **439**, 321 (1997).
[17] P. Hanh *et al.,* J. Appl. Phys. **51**, 2079 (1980).
[18] M. V. R. Murty *et al.* (to be published).
[19] S. K. Sinha *et al.,* Phys. Rev. B **38**, 2297 (1988).
[20] Surface reconstruction changes the specular beam intensity by less than 1% at the $(0\ 0\ 0.18)_{\text{hex}}$ position.
[21] J. A. Stroscio *et al.,* Phys. Rev. Lett. **75**, 4246 (1995).
[22] J. Villain, J. Phys. I (France) **1**, 19 (1991).
[23] M. D. Johnson *et al.,* Phys. Rev. Lett. **72**, 116 (1994).
[24] W. C. Elliot *et al.,* Phys. Rev. B **54**, 17 938 (1996); F. Tsui *et al.,* Phys. Rev. Lett. **76**, 3164 (1996); L. C. Jorritsma *et al.,* Phys. Rev. Lett. **78**, 911 (1997).
[25] J. G. Amar and F. Family, Phys. Rev. Lett. **77**, 4584 (1996); S. C. Wang and G. Ehrlich, Phys. Rev. Lett. **70**, 41 (1993).
[26] J.-K. Zuo and J. F. Wendelken, Phys. Rev. Lett. **78**, 2791 (1997).
[27] T. Curcic *et al.* (unpublished).
[28] J. W. Evans *et al.,* Phys. Rev. B **41**, 5410 (1990).
[29] J. G. Amar and F. Family, Phys. Rev. B **54**, 14 742 (1996).
[30] A plausible explanation for the shorter period during sputtering is a coordination dependent sputter yield Y with Y higher near step edges. However, this is unlikely because measurement of the average island separation during sputtering at 120 °C indicates that a fivefold increase in sputter yield (for ions striking within two lattice sites of a step) is required to account for the shorter period. We have also determined that during simultaneous growth and irradiation [see Fig. 1(b)] we are not in a step flow/retraction regime due to a reduced flux of adatoms/vacancies. A slight imbalance in the deposition rate or the ion flux results in intensity oscillations. The period is defined here as the time between successive maxima in the specular beam intensity.
[31] M. C. Bartelt and J. W. Evans, Phys. Rev. Lett. **75**, 4250 (1995).
[32] J. Tersoff, A. W. D. van der Gon, and R. M. Tromp, Phys. Rev. Lett. **72**, 266 (1994).